Experimental Study On The Crack Resistance Of Expansive Soil Stabilized With Water-Soluble Polymers

Hang Tan[1], Liang Zhou[2*], Xumin Wang[1], Yongxia Liu[3], and Yunlong Jia[1]

[1] School of Civil Engineering, Architecture and Environment, Hubei University of Technology, Wuhan, 430068, China
[2] Lanzhou Bowen College of Science and Technology, Lanzhou, 730101, China
[3] Gansu Tieke Construction Engineering Consulting Co., Ltd. Lanzhou, 730030, China
[*] Corresponding author. E-mail: 2640108581@qq.com

Received: Sep. 28, 2025; Accepted: Mar. 24, 2026

This study examines the impact of sodium polyacrylate (PAAS) on crack resistance in expanded soil subjected to hydraulic erosion, addressing the issue of multiple cracks and strength degradation in this soil type. The findings indicated a 63.56% decrease in the liquid limit and a 92.62% decrease in the plasticity index of the stabilized soil. Additionally, the free expansion ratio decreased to 19.58%. As the PAAS content increased, the expansion ratio decreased by 34% to 57% for no load and by 35% to 93% for load. The initial rise in compressive strength of stable soil is followed by a decline as PAAS content increases. Optimal results are observed at a 4% dosage. Likewise, the deformation modulus initially increases and then decreases, peaking at an 88.93% enhancement. The stabilized soil's maximum shear strength reached 216.02 kPa , marking a 261.78% increase compared to untreated soil, which coincided with a 112.46% rise in cohesion and a 137.74% increase in the internal friction angle. The compressive strength, cohesion, and angle of the stabilized soil decreased as the number of wet-dry cycles increased. The decrease slowed down after four cycles. X-ray diffraction (XRD) analysis revealed no formation of new minerals post PAAS treatment, with a 43.14% decrease in hydrophilic minerals. Furthermore, a gelation film with adhesive properties was formed, effectively restraining soil crack expansion.

Keywords: Expansive soils; PAAS, Expansion Characteristics; Mechanical Properties; Dry and Wet Cycles; Microscopic Mechanisms

http://dx.doi.org/10.6180/jase.202609_32.034

1. Introduction

Expansive soil, as a special type of clay, exhibits significant changes in swelling when absorbing water and shrinking when losing water. It mainly contains hydrophilic clay minerals such as montmorillonite, illite, and kaolinite [1, 2]. Its swelling and shrinking characteristics, along with its highly fractured nature, lead to reduced soil bearing capacity and uneven settlement of pavements, resulting in common engineering issues like cracking and subsidence of road surfaces. This greatly diminishes road performance and can pose serious hazards to people's safety, which is why expansive soil is also referred to as 'the cancer of the engineering world' [3]. Research shows that in areas with expansive soil, the construction of railway subgrades results in over 70,000 annual defects and more than 8,000 km of damaged lines, with a subgrade damage rate as high as 75%. Therefore, before carrying out road engineering in expansive soil areas, it is necessary to reinforce the expansive soil to reduce its swelling and shrinkage and improve its strength to meet the safety requirements of the construction project.

Studies have shown that using traditional cement, lime,

Table 1. Basic physical parameters of expansive soil

Natural moisture content /%	Optimal moisture content /%	Maximum dry density /(g/cm^3)	Liquid limit /%	Plastic limit /%	Plasticity index	Free expansion rate /%
22.04	20.3	1.76	42.54	11.09	31.45	43.1

and alkali slag can improve the mechanical properties of expansive soil and reduce its expansiveness [4–6]. However, traditional stabilizers result in higher early strength and have a significant impact on the surrounding environment. To address the shortcomings of traditional stabilizers, researchers have introduced biopolymers to stabilize expansive soil. Studies indicate that adding biopolymers can significantly enhance the strength of expansive soil, form a gel that makes the soil particles more compact, and inhibit crack development in the early stages [7–10]. Nevertheless, biopolymers are easily soluble in water, and the effects vary depending on the mixing method, making them sensitive to how they are mixed, and their ability to inhibit crack development in later stages is relatively limited. Some scholars have shown that through microbially induced calcium carbonate precipitation, as the amount of cementing solution increases, the shear strength of solidified expansive soil gradually improves, and the compression deformation gradually decreases [11–13]. However, experiments using microbially induced calcium carbonate precipitation are complex, require high maintenance of the bacterial solution, and are costly, which is not conducive to conducting the experiments.

Studies have shown that water-soluble polymers can effectively improve the mechanical properties, stability, and durability of soil [14, 15]. Research indicates that the addition of water-soluble polyurethane effectively inhibits the water absorption swelling and water loss shrinkage characteristics of expansive soil, enhancing the soil's stability and bearing capacity [16, 17]. Studies have shown that the addition of polyacrylamide significantly increases the soil's compressive and shear strength while also reducing its permeability and compressibility [18, 19]. Research has found that new polymers can significantly enhance the mechanical properties of soil and reduce its environmental sensitivity [20–22]. To this end, it is particularly important to innovatively introduce high polymer polymers, especially the environmentally friendly material sodium polyacrylate (PAAS), for the reinforcement treatment of expansive soil, in order to compensate for the shortcomings of traditional stabilizers. PAAS itself is a highly water-absorbent resin, inexpensive, and as a chemical modifier, it has been recognized as an environmentally friendly soil stabilizer. It is a non-toxic, water-soluble polymer containing a large number of hydrophilic groups such as carboxyl and hydroxyl groups. It has been used as a thickener in the food industry and a flocculant in water treatment. Due to its low cost and resistance to microbial degradation, it has been widely applied in the stabilization of concrete, red clay, and bentonite [23, 24]. PAAS has the unique properties of high water absorption and high viscosity, and demonstrates more significant effects in the solidification of cement, bentonite, and red clay, particularly excelling in enhancing the bearing capacity of solidified expansive soil and resisting soil deformation [23–25]. Studies have shown that sodium polyacrylate has achieved remarkable results in the solidification of expansive soil, providing strong support for its application in the reinforcement of expansive soil [25]. Wang et al. [23] found that after sodium polyacrylate solidifies red clay, the shear strength first increases and then decreases with varying content, reaching a peak at a content of 2%. Chen et al. [24] indicates that after PAAS solidifies bentonite, a complete layered structure forms within the soil, and the interlayer spacing of montmorillonite is significantly reduced. As a highly absorbent water-soluble resin, PAAS exhibits a unique soil improvement effect due to its rich carboxyl groups and excellent hydrophilic polymerization properties [26]. In recent years, research on the use of PAAS in soil stabilization has gradually increased, and studies have found that the addition of PAAS significantly enhances the compressive and shear strength of soil while reducing its permeability and compressibility.

In summary, the use of PAAS with high water absorption regulates the effective water content within the soil, reducing volumetric expansion and contraction caused by wet-dry cycles. Simultaneously, its cross-linked structure forms an 'elastic-rigid' composite framework with soil particles, which can enhance the deformation capability and increase the strength of the stabilised soil, addressing the brittleness and cracking issues associated with traditional stabilisers. Mechanical tests analyse the mechanical behaviour and deformation resistance of PAAS-stabilised expansive soil. Swelling tests examine the expansion and contraction behaviour, and wet-dry cycle tests study changes in soil water content and crack characteristics. Scanning electron microscopy (SEM) and X-ray diffraction (XRD) tests reveal the interface mechanisms between hydrogel formed by

Table 2. PAAS basic physical properties

Material	molecular weight g/mol	Granularity $/mesh$	pH	300 °C	Viscosity dL/g
PAAS	10 million	200∼400	7.8	Do not decompose	0.060∼0.10

PAAS and soil particles, the changes in porosity and mineral composition of stabilised expansive soil, constructing an intrinsic mechanism of 'macroscopic effects-microscopic mechanisms' interaction. This provides a theoretical basis for the construction of subgrades and slope projects in soft expansive soil areas, enriches the theory of expansive soil stabilisation, and proposes a new method for management that balances ecological protection with performance improvement.

2. Materials and methods

2.1. Materials used in the test

The sample soil was taken from a road construction project in Huanggang City, Hubei Province, with a collection depth of 1.5 meters. The soil is grayish white, and it is hard and plastic in natural state. Before the test, the soil was dried naturally, and the final moisture content reached 22.04%. Then, the professionals carefully removed the impurities in the soil and crushed them through a 2 mm sieve for subsequent analysis.

As shown in Fig. 1, the particle size distribution curve shows that 90% of soil particles are less than 0.075 mm, which makes it classified as fine-grained soil according to the existing classification criteria. Table 1 systematically summarizes the physical properties of expanded soil. It is worth noting that the Uniformity Coefficient (Cu = 2.98) and the Curvature Coefficient (Cc = 0.13) indicate that the soil has poor grading [27]. In addition, this soil is classified as weakly expanded soil, which exhibited a liquid limit of 42.54% and a free expansion index of 43.1% [27].

The curing agent used in the experiment is industrial-grade PAAS, sourced from Tianjin Huasheng Chemical Reagent Co., Ltd. It is a colorless, odorless white powder with the structural formula [-CH2 − CH(COONa) −]n. The basic physical parameters are shown in Table 2, and the particle size distribution is shown in Fig. 1.

It has advantages such as high water retention, non-toxicity, and environmental friendliness, and is a water-soluble polymer. Its viscosity changes very little, it is not prone to deterioration, is unaffected by temperature or acid, alkali, and salts, although strong alkali can increase its viscosity.

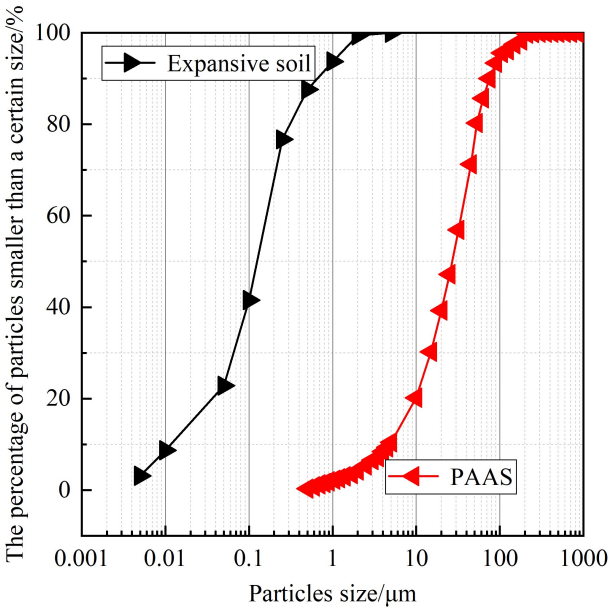

Fig. 1. Particle size curve of expansive soil and PAAS

2.2. Sample Preparation and Test Methods

In the experiment, the clay-soil ratio of PAAS to expansive soil was 0%, 0.5%, 1%, 2%, 3%, 4%, and 5% (Currently, there is no unified standard stipulating that the maximum PAAS content in stabilized expansive soil must be 5%. Relevant studies on stabilized expansive soil consider it reasonable to set the maximum PAAS content at 5% [24], as exceeding this content significantly reduces the cost-effectiveness of the treated soil), with curing times of 0d, 7d, 14d, 28d, and 60d. All experiments in the text were conducted in accordance with standard [27]. Three parallel samples were set for each test group and their average values were taken.

2.2.1. Experimental Sample Preparation Steps

(1) First, determine the maximum dry density and the optimum water content of the expansive soil based on the compaction test. Then, using the maximum dry density and the optimum water content, take the reserved expansive soil and pure water. The clay content ratio is set at 0%, 1%, 2%, 3%, 4%, and 5% (percentage of sodium polyacrylate powder by mass of expansive soil).

(2) After preparing the expansive soil (as shown in Fig. 2a) and sodium polyacrylate powder (as shown in Fig. 2b) and mixing them thoroughly in dry form, gradu-

ally add pure water multiple times (as shown in Fig. 2c) and stir until a clearly visible mixture is formed.

(3) Pour the mixture from (2) into standard molds with a height of 100 mm and a diameter of 50 mm (as shown in Fig. 2h , for compressive strength tests and microscopic tests), and molds with a diameter of 61.8 mm and a height of 200 mm (as shown in Fig. 2g, for direct shear tests, swelling tests, and wet-dry cycle tests). The load applied for static loading in one-time static pressing is 1.5 MPa. After holding the static pressure for 2 minutes, remove the load and take out the specimens, wrap them with plastic wrap, and place them in a curing room (temperature approximately $25°C \pm 2°C$, humidity approximately $40\% \pm 5\%$). Conduct tests after curing for 0, 7, 14, 28, and 60 days.

Fig. 2. Experimental flow

2.2.2. *Test Method*

(1) Free expansion rate test

A free swelling test was conducted to simulate the soil's free water absorption and swelling characteristics under conditions without external forces or lateral constraints. The test steps are as follows:

(i) Slowly pour the pre-weighed 10 g soil sample into a glass funnel, ensuring the soil is evenly distributed inside the funnel to prevent clumping. Quickly remove the conical stopper, allowing the soil to fall freely into the 50 mL measuring cylinder below. After all the soil has fallen and no particles are moving, record the soil's bulk volume to the nearest 0.1 mL. Slowly add distilled water into the cylinder containing the dry soil until the water level is 10 mm above the soil surface, pouring along the side of the cylinder to avoid disturbing the soil.

(ii) Gently stir the soil sample and water in the measuring cylinder with a glass rod, stirring to a depth approximately to the bottom of the soil sample, at a stirring rate of 1 time/s for 1 minute, ensuring the soil sample is fully moistened. After stirring, let the measuring cylinder stand (as shown in Fig. 2d) to allow the soil sample to freely absorb water and swell, preventing the measuring cylinder from shaking during the standing period. Record the volume of the swollen soil sample at 10 minutes, 30 minutes, 1 hour, 2 hours, 4 hours, 8 hours, and 24 hours of standing, until the difference between two consecutive readings does not exceed 0.1 mL, at which point the volume is considered the stable swollen volume.

(2) Limit Moisture Content Test

Prepare no less than 200 g of soil samples that have passed through a 0.5 mm standard sieve and remove coarse particles. Divide the 200 g of soil into three portions, each approximately 60 $\sim$ 70 g, and add different volumes of distilled water to prepare soil pastes in three states: slightly dry, medium, and slightly wet. Seal the three soil pastes and let them stand for 12$\sim$24 hours to ensure uniform moisture distribution. Then perform the liquid-plastic test using a photoelectric liquid-plastic limit tester (as shown in Fig. 2e), with a 76 g cone for the cone penetration. The water content at a cone penetration of 17 mm is the liquid limit, and the water content at a cone penetration of 2 mm is the plastic limit.

(3) Compaction Test

The light compaction test is used (as shown in Fig. 2f). Before the test, the designed proportions of expansive soil and sodium polyacrylate are mixed. They are then prepared into five portions with a 2% incremental moisture content difference, and each portion is cured for 24 hours before compaction (in three layers) to determine the maximum dry density and the optimum moisture content.

(4) Swelling Rate Test

The swelling rate without load and with load is measured using a single rod consolidometer (as shown in Fig. 2i). The changes in the dial gauge are recorded at regular intervals until the dial gauge stabilizes and no longer changes.

(5) Compressive Strength Test

The test is conducted using a WDW-10E microcontrolled electronic universal testing machine (as shown in Fig. 2l), with a loading rate of 1.2 mm/min. The test should be stopped when a clear peak appears on the stress-strain curve or when the stress stabilizes. If there is no obvious peak, the test should be stopped when the strain reaches 20%.

(6) Shear Strength Test

The test was conducted using a ZJ-type strain-controlled direct shear apparatus produced by Nanjing Soil Instrument Factory (as shown in Fig. 2j). The shear rate was 0.8 mm/min, and the normal stresses were 100 kPa, 200 kPa, 300 kPa, and 400 kPa. A shear load was applied to

the sample until complete failure, and the shear stress and shear displacement of the sample were recorded.

(7) Dry-Wet Cycling Test

To simulate the characteristics of cracks under atmospheric precipitation, the specimen along with the ring knife/mould is placed in a water container, with the water level controlled at 1/3 to 1/2 of the specimen height, allowing water to infiltrate from bottom to top to ensure uniform moisture content, with a single humidification period of 6 hours. Afterwards, the specimen (same as the shear specimen) is placed in a 40 °C constant temperature electric drying oven (as shown in Fig. 2k) to dry, with a single drying period of 24 hours. After the wet-dry cycles, images of the surface cracks of the specimen are captured, and the crack length and width are extracted, completing a total of 5 wet-dry cycles.

(8) Microscopic Test

During the test, samples from the compressive strength test were selected, broken into roughly 1 mm cubic pieces, then freeze-dried (using a liquid nitrogen freeze dryer), dried, ground, and sieved through a 0.075 mm mesh, and kept sealed for later use. The reserved soil samples were attached to conductive tape and vacuum freeze-dried to reduce disturbances in the sample's charge and discharge. They were then tested using a HITACHI field emission scanning electron microscope (as shown in Fig. 2m) with a resolution of 1.0 nm(15kV)/1.3nm(1kV) and a voltage range of $0.1 - 30$kV.

Soil from the center of the compressive test samples was placed in a 50 °C oven to dry. After drying, the soil samples were ground, sieved through a 0.075 mm mesh, and stored in sealed bags for later use. XRD tests were conducted using an Ultima IV X-ray diffractometer (as shown in Fig. 2n), with X-ray diffraction analysis showing linearity ≤ 0.030, resolution ≤ 0.130, repeatability ≤ 0.0020, scanning angle $10^\circ - 80^\circ(2\theta)$, a scan step of 0.02, and a speed of 5°/min.

3. Result discussions

3.1. Effect of PAAS on the boundary moisture content of solidified soil

Figs. 3a and 3b illustrate the boundary moisture content of solidified soil after 0 days and 60 days of curing, respectively. As shown in Fig. 3a, with an increase in PAAS content, both the liquid limit and plasticity index exhibit a gradual decline. The extent of this decrease shifts from significant to relatively minor, eventually approaching a stable trend [25]. Specifically, when the PAAS dosage reached 5%, the liquid limit of the solidified soil dropped to 20.36%, and the plasticity index decreased to 7.12%, representing reductions of 52.14% and 77.36%, respectively, compared to the uncured soil. Conversely, the plastic limit of the solidified soil increased progressively with higher PAAS dosages, although the magnitude of this increase was relatively small. The rate of increase gradually diminished and eventually stabilized. At a 5% dosage, the plastic limit reached 13.24%, marking a 19.39% increase over the uncured soil.

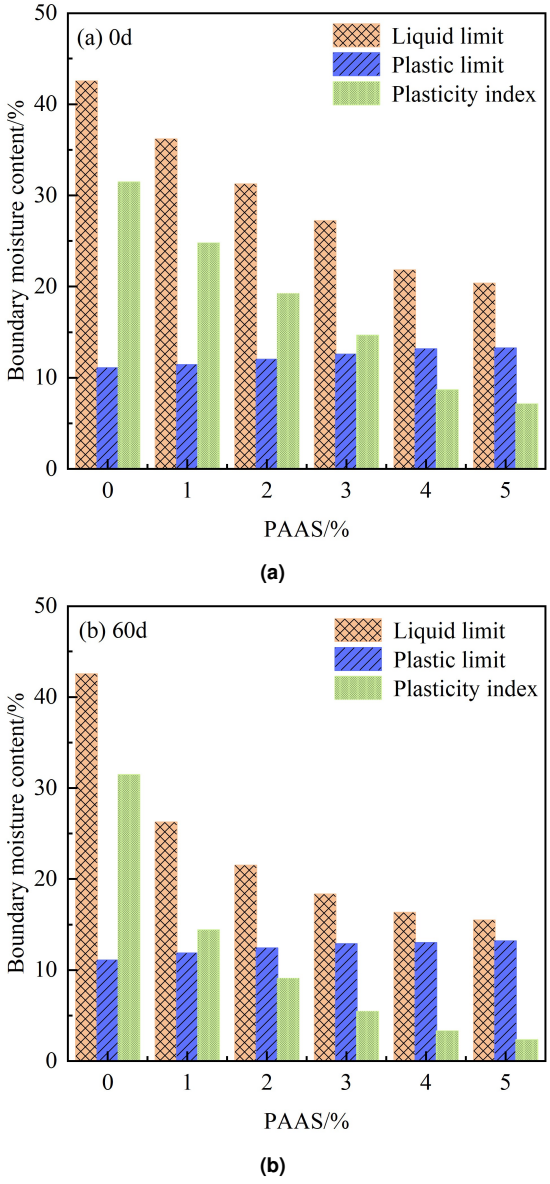

Fig. 3. Water content of cured soil boundaries

Fig. 3b reveals that the trends in liquid limit, plastic limit, and plasticity index of the soil subjected to 60 days of curing exhibit similarities to those of the uncured soil. Nevertheless, when compared with the 0 -day curing sample, the reductions in both the liquid limit and plasticity index of the 60-day-cured soil are notably more pronounced. Specif-

ically, the data indicates that the liquid limit and plasticity index have decreased by 63.56% and 92.62%, respectively. Moreover, relative to the uncured soil, the rates of reduction have increased by 11.42% and 15.26%, respectively.

This is attributed to the strong water-absorbing property of PAAS-the higher the dosage, the more water PAAS absorbs from the soil, leading to thinner bound water films and a reduced plasticity index. Moreover, PAAS requires a prolonged hydration process, resulting in a lower plasticity index for the 60-day-cured soil compared to the 0-day sample [28].

3.2. Effect of PAAS on the swelling properties of solidified soils

3.2.1. Effect on the rate of free expansion

Figs. 4a and 4b respectively depict the free expansion ratios of solidified soil under varying dosages and different curing durations. As depicted in Fig. 4a, under identical curing durations, the free expansion rate of the solidified soil demonstrates a declining trend with the increase in PAAS content. In accordance with specification [29], the free expansion rate of 5% solidified soil over a 60-day duration is recorded at only 19.58%, representing a substantial decrease of 53.82% relative to uncured soil, with its rate being considerably below the 40% threshold, thereby excluding it from the expansive soil classification. As depicted in Fig. 4b, under a given PAAS content, the free expansion rate of solidified soil exhibits a declining trend over time, with a significantly greater reduction in the swelling rate when the PAAS content exceeds 4%.

3.2.2. Effect of PAAS on unloaded expansion rate

Figs. 5a and 5b respectively illustrate the unloaded expansion rates of solidified soil with varying additive amounts and different curing durations. Fig. 5a indicates that for a given curing period, the unloaded expansion rate is inversely related to the additive dosage, at a diminishing rate of decrease. Specifically, for 5% cured soil, the unloaded expansion rate drops by 36.22 %, 44.76 %, 47.41 %, 52.08 %, *and*56.37 %, respectively. Fig. 5b reveals that, with a constant additive amount, the unloaded expansion rate of the solidified soil declines over time. After 60 days of curing, the unloaded expansion rates of the cured soil decrease by 34.22 %, 44.76 %, 50.85 %, 53.96 %, and 56.37 %, respectively. However, when the additive content reaches 4%, the reduction in the unloaded expansion rate becomes less significant. Therefore, considering both the additive dosage and curing effect of PAAS, the 4% solidified expansive soil exhibits the optimal performance in terms of expansion rate.

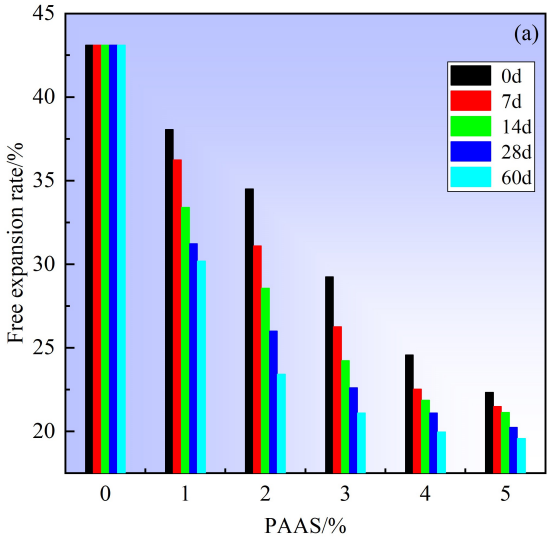

(a) Different dosages

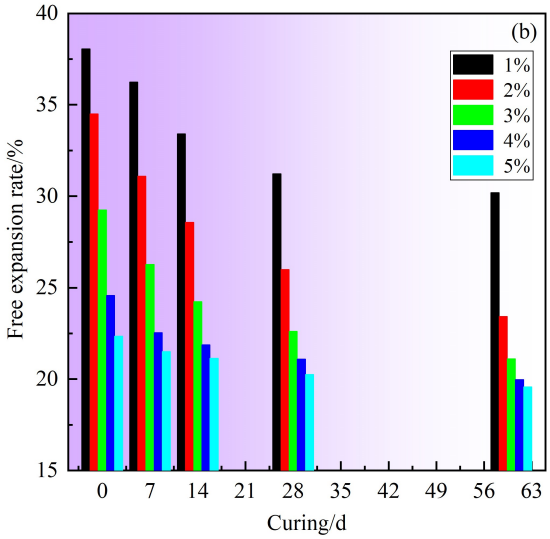

(b) Different curing periods

Fig. 4. Free expansion rate of cured soil

3.2.3. Effect of PAAS on the rate of expansion of the charge

Figs. 6a and 6b respectively depict the loaded expansion rates of solidified soil under a pressure of 50 kPa for different additive dosages and curing durations. As illustrated in Fig. 6, the trend of the loaded expansion rate with additive content and curing time closely parallels that observed for the unloaded case. Fig. 6a demonstrates that the load expansion rate declines swiftly before the additive dosage reaches 4%, after which the rate of decrease slows down. Specifically, for solidified soil cured for 60 days, the load expansion rate decreases by 35.95 %, 65.53 %, 81.84 %, 89.22 %, and 92.81 %, respectively, with reduction rates ranging between 35% and 93%. According to Fig. 6b, the extent of

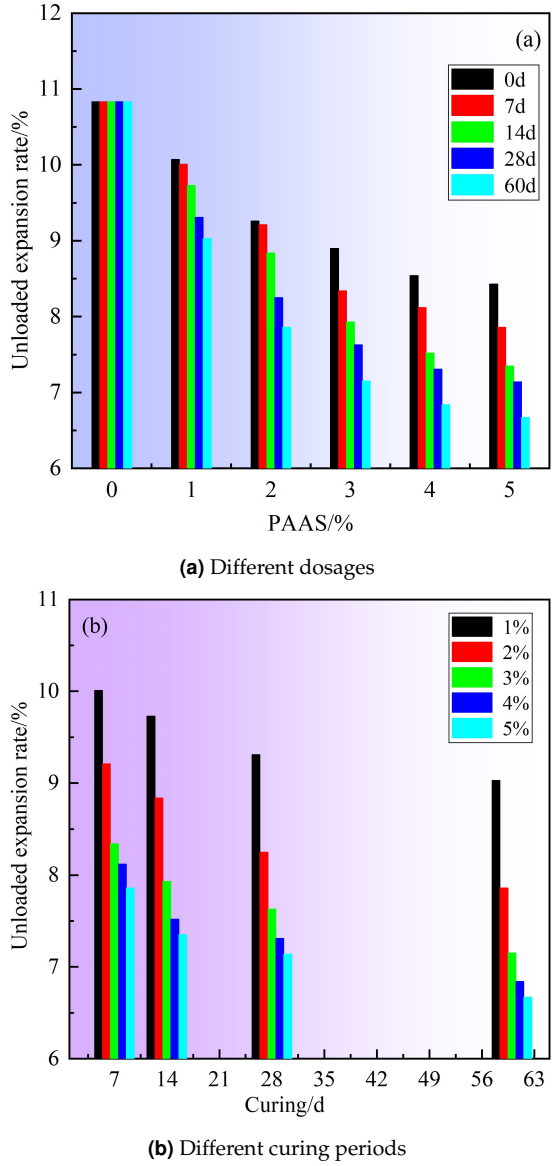

(a) Different dosages

(b) Different curing periods

Fig. 5. Unloaded expansion rate of cured soil

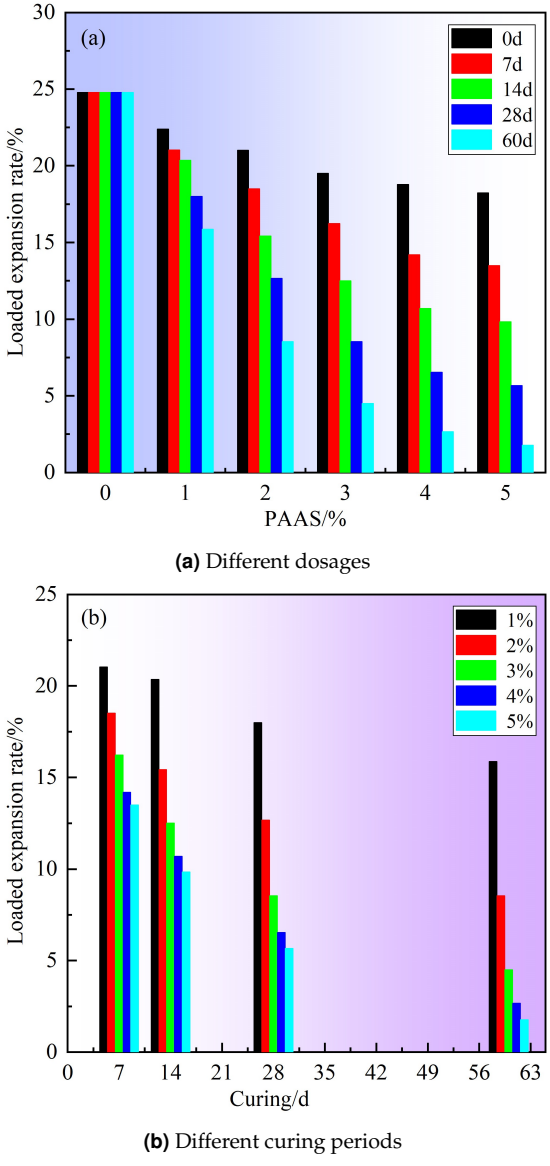

(a) Different dosages

(b) Different curing periods

Fig. 6. Loaded expansion rate of cured soil

reduction is more pronounced during the initial 28 days of curing, suggesting that after a certain curing period, the internal structure of the solidified soil gradually stabilizes, leading to a slower rate of reduction.

3.3. Effect of PAAS on compressive strength

Figs. 7a and 7b respectively present the compressive strength of solidified soil under varying additive dosages and curing periods. In Fig. 7a, at a consistent curing time, an initial rise followed by a decline is observed in the compressive strength of the solidified soil as additive content increases. The peak compressive strengths recorded were 148.36 kPa, 178.58 kPa, 205.36 kPa, 242.23 kPa, and 291.74 kPa (at a 4% dosage), representing increases of 47.21 %, 50.92 %, 52.97 %, 55.79 %, and 60.68 %, respectively, compared to the un-cured state (across different curing durations). Moreover, under a constant additive dosage, a gradual increase over time, leading to a stable state, is observed in the compressive strength of the solidified soil.

Fig. 7b reveals that the compressive strengths of soil samples subjected to a 60-day curing period with varying additive dosages are 114.7 kPa, 172.23 kPa, 239.68 kPa, 264.74 kPa, 291.58 kPa, and 277.61 kPa, respectively. These values demonstrate increases of 31.76%, 43.31%, 111.07%, 101.2%, 96.64%, and 104.93% compared to their un-cured counterparts.

The compressive strength gain is primarily due to the water absorption and adsorption properties of PAAS. Upon

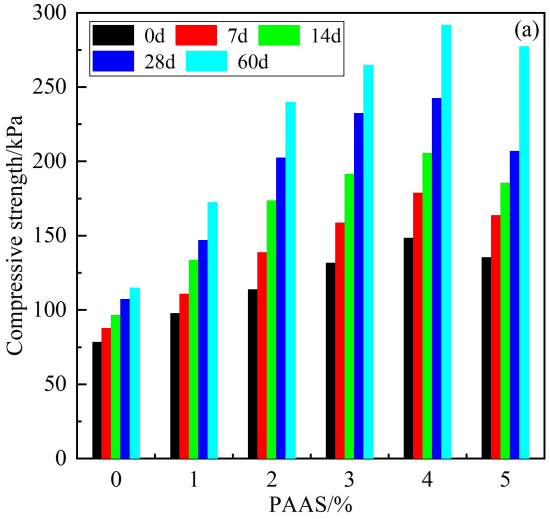

(a) Different dosages

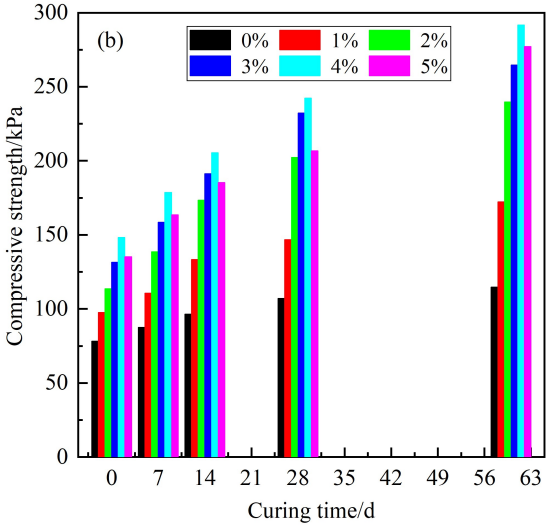

(b) Different curing periods

Fig. 7. Compressive strength of cured soil

absorbing water and expanding, PAAS forms a gel-like substance that strengthens the inter-particle bonds within the soil, fills the voids between particles, and enhances the soil's compactness, thereby boosting its compressive strength. As the curing time progresses, PAAS absorbs water more thoroughly, generating additional gel that further connects the soil particles and subsequently elevates the compressive strength.

The deformation modulus E_{50} serves as a widely recognized metric for forecasting the deformation behavior of solidified soils, reflecting the material's capacity to withstand elastoplastic deformation [29].

Fig. 8 illustrates the correlation between the deformation modulus E_{50} and the PAAS curing agent. As depicted, under varying curing durations, the E_{50} value of the solidified soil rises and subsequently declines, reaching its peak at a 4% dosage level. Specifically, the peak E_{50} values at 0 days, 7 days, 14 days, 28 days, and 60 days of curing were 26.02 MPa, 29.76 MPa, 33.03 MPa, 63.29 MPa, and 62.07 MPa, respectively (all at a 4% content). These findings indicate that the solidified soil's resistance to deformation significantly enhances after prolonged curing, with a maximum improvement of 88.93%.

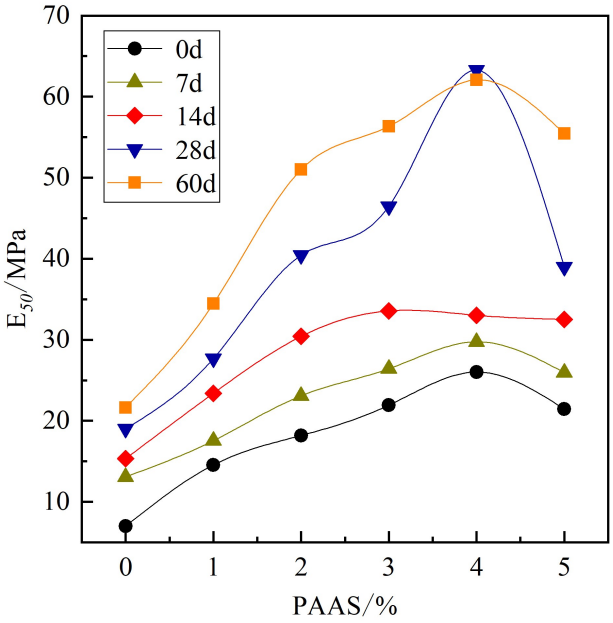

Fig. 8. Relationship between changes in E_{50} and PAAS

3.4. Effect of PAAS on shear strength

Figs. 9a and 9b respectively present the shear strength of solidified soil after curing periods of 0 days and 60 days. As evident from Fig. 9, the shear strength exhibits a linear increase with the augmentation of normal stress. Moreover, as the curing time extends, the shear strength experiences a progressively greater rise. After 60 days of curing with a 4% content, the maximum shear strength reached 216.02 kPa, marking a 261.78% increase compared to the uncured soil (59.71 kPa). This indicates a substantial enhancement in shear strength post-curing. Notably, the shear strength increases at a slower rate under normal stress below 200 kPa (low stress conditions), whereas it escalates rapidly under normal stress exceeding 200 kPa (high stress conditions).

Fig. 9a shows that, at 0 days of curing, the soil treated with 3% PAAS exhibits the highest shear strength. This is because PAAS is a water-soluble polymer with numerous polar groups along its molecular chains. When the dosage reaches 3% (well above the conventional 'effective

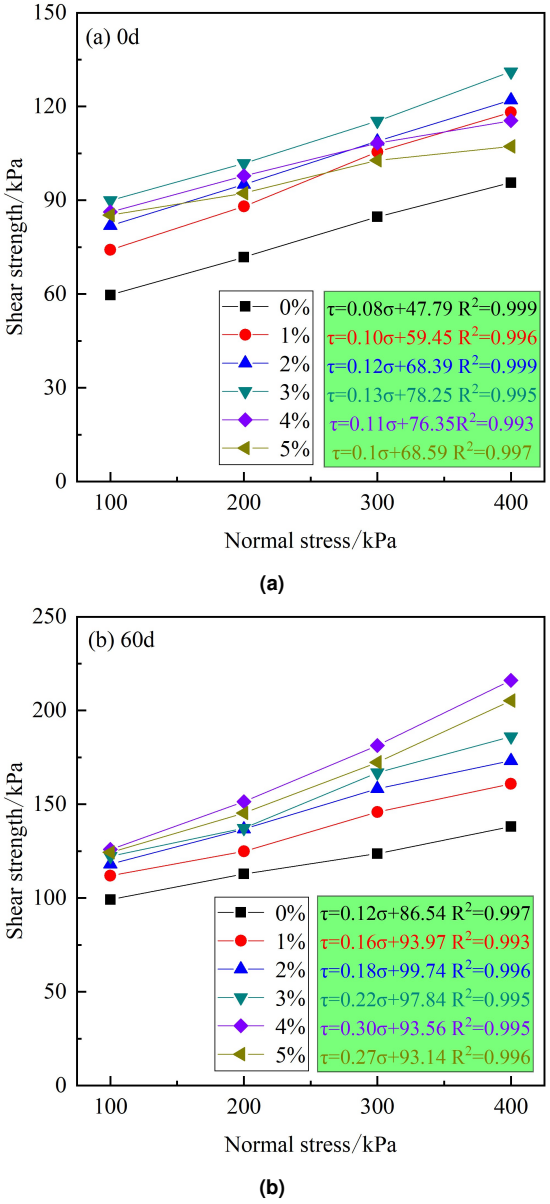

Fig. 9. Shear strength of cured soil

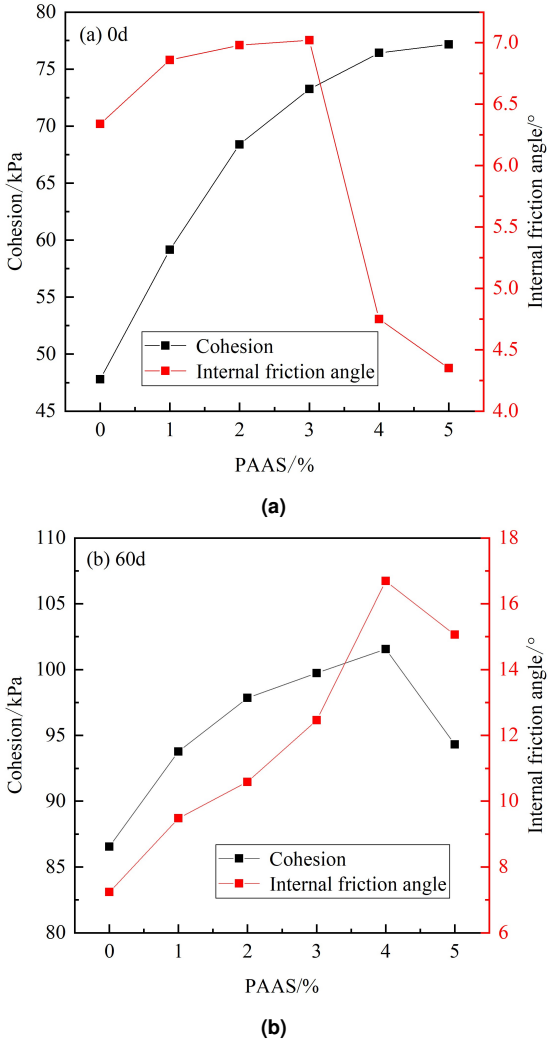

Fig. 10. Cohesion and angle of internal friction of cured soil

active component range of 0.8 ∼ 1.2%'), PAAS forms a 'high-concentration aqueous environment' in the soil. Water molecules act as a medium, allowing the PAAS chains to quickly expand and adsorb onto the surfaces of expansive soil particles. The instantaneous physicochemical effects of PAAS on expansive soil dominate the early strength development at zero curing. The increase in soil shear strength does not rely on the hardening from hydration reactions of conventional cementitious materials (which takes days to tens of days), but rather on the rapid physical encapsulation, ionic complexation, and pore filling between PAAS molecules and expansive soil particles. Furthermore, the 3% dosage precisely brings these three effects to a 'synergistic peak.'

Figs. 10a and 10b respectively display the cohesion and internal friction angle of the curing soil after curing periods of 0 days and 60 days. As depicted in Fig. 10, the internal friction angle of the solidified soil peaks and then declines with additional increases in content, showing a fundamental alignment with the trend observed in the uncured soil. Specifically, Fig. 10 reveals that the peak internal friction angles before and after curing are achieved at 3% and 4% contents, measuring 7.02° and 16.69°, respectively. This indicates a 137.74% increase in the internal friction angle following curing. Furthermore, the cohesion of the uncured soil at 0 days of curing gradually rises with an increase in PAAS content, eventually stabilizing at 77.16 kPa at a 5% content. This represents a 61.42% rise compared to the co-

hesion (47.8 kPa) of the uncured soil at the initial curing stage (0 days).

Following a 60-day curing period, the soil cohesion initially rose and subsequently declined as the PAAS content increased. The maximum cohesion value reached 101.56 kPa, marking a 112.46% increase compared to the uncured state. This phenomenon can be attributed to the gel formation resulting from PAAS absorption and expansion, which bolsters the cohesion between soil particles.

Meanwhile, the substantial water-absorbing capacity of PAAS causes a decrease in soil moisture content, thereby reinforcing the bonding forces and frictional resistance among soil particles, and resulting in an upsurge in the internal friction angle. Nevertheless, an overabundance of gel interspersed among soil particles can adversely affect soil structure, diminish interparticle cohesion, and consequently, reduce shear strength.

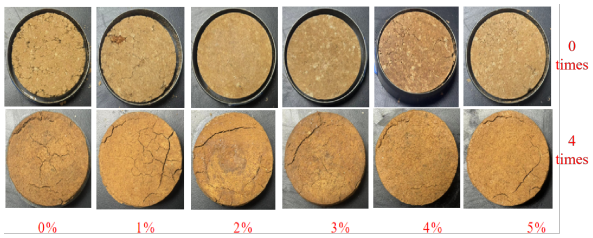

Fig. 11. Dry and wet cyclic crack changes

3.5. Effect of wet-dry cycles on cracks

In regions where expansive soil is distributed, the soil undergoes multiple wet-dry cycles throughout the year due to the influence of monsoon climates or seasonal rainfall. During the rainy season, water infiltrates the soil, making it wet and causing it to swell, while in the dry season, solar radiation leads to moisture evaporation, causing the soil to dry and shrink. This alternation occurs 4-6 times annually. Five wet-dry cycles can accurately simulate the year-round wet-dry process of expansive soil subgrades, slopes, and other engineering projects under natural atmospheric conditions, reflecting the typical climatic effects encountered during actual use. After stabilizing expansive soil with sodium polyacrylate, the repeated increase and decrease of moisture during wet-dry cycles gradually destroys the internal structure of the soil, leading to a continuous decline in its strength. This decrease in strength does not continue indefinitely. Studies have shown that the decline is significant during the early cycles, but after 4-5 cycles, the rate of strength reduction slows noticeably and tends to stabilize. Wet-dry cycle tests on sodium polyacrylate-stabilized expansive soil show that when the cycling amplitude is 10% – 35%, the soil's cohesion and other strength parameters stabilize after five cycles. Continuing to increase the number of cycles results in minimal changes in strength. Setting the number of cycles to five can accurately capture the complete process of stable soil from performance degradation to stabilization, which is sufficient to assess its long-term stability while avoiding issues of too few cycles failing to reflect true performance or too many cycles extending the test period and increasing costs.

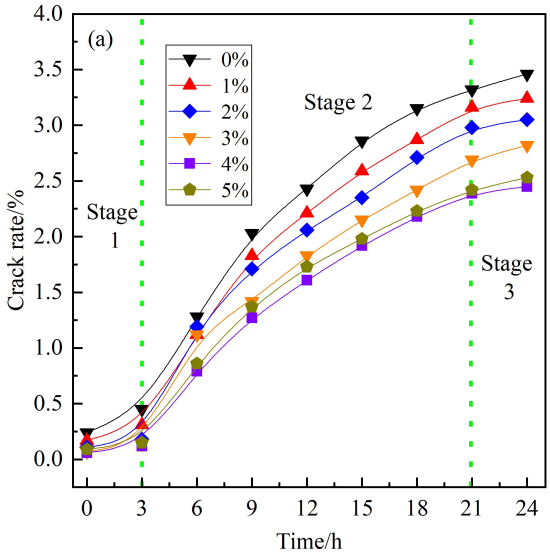

(a) 1 cycle

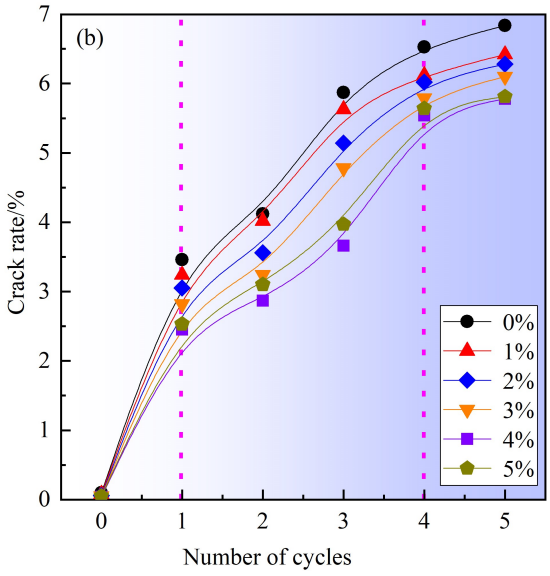

(b) Number of cycles

Fig. 12. The crack rate of solidified soil under the action of dry and wet cycles

Fig. 11 respectively illustrate the crack ratios (Refers to the percentage of the total area of all cracks on the sample

surface or cross-section relative to the total observed area) of solidified soil after a single cycle and multiple cycles. It is evident that, prior to any cyclic loading (0 cycles), the solidified soil specimen undergoes significant shrinkage deformation, with the soil edges progressively detaching from the ring knife. As the PAAS content increases, this shrinkage deformation gradually diminishes, with a minor portion of the specimen's deformation at a 4% PAAS content approaching the constraints of the ring knife. Following four cycles, surface branching cracks on the solidified soil begin to progressively widen and penetrate deeper, ultimately segmenting the soil into several distinct sections.

As the content of PAAS increases, both the crack width and the number of cracks significantly decrease, indicating that the addition of PAAS effectively suppresses crack development. Notably, when the PAAS content reaches 4%, the crack rate drops to its lowest level, demonstrating the optimal inhibitory effect on crack propagation at this concentration. The underlying mechanism involves the water-absorbing property of PAAS, which reduces the soil's free water content and hinders the interaction between hydrophilic clay minerals and water. This, in turn, diminishes soil swelling and minimizes the formation of interlayer cracks in the soil Error! Reference source not found.. Furthermore, the hydroxyl (-OH) and carboxyl (-COOH) groups in PAAS molecules can form hydrogen bonds with clay minerals, creating a stable three-dimensional structure. This structural reinforcement enhances the soil's tensile strength and consequently improves its crack resistance.

Fig. 12 illustrates the crack ratio of the solidified soil subjected to dry-wet cycling. As depicted in Fig. 12a, the evolution of the crack ratio can be divided into three primary phases [10]: Initially, there is a rapid growth phase ($0 \sim 3$ h), where stress concentrations arising from soil inhomogeneity trigger the formation of numerous cracks. Subsequently, a slow growth phase ($3 \sim 21$ h) ensues, during which new cracks emerge along pre-existing ones, resulting in a progressive rise in the crack ratio. Finally, a stable phase ($21 \sim 24h$) is reached, wherein, once the cracks have propagated to a certain extent, the soil's tensile resistance surpasses its tensile capacity, causing crack development to cease.

As illustrated in Fig. 12a, during the initial stage, there exists only a marginal disparity in the crack rates between solidified and unsolidified expansive soils. However, in the subsequent stage, the gap between their crack rates widens significantly, with the crack rates for 0% and 4% solidified soils recorded at 3.46% and 2.45%, respectively. The difference in their crack rates amounts to 29.19%, underscoring that PAAS primarily acts to inhibit the cracking of expansive soil during the second stage.

Furthermore, Fig. 12b reveals that the relationship between the crack rate and the number of dry-wet cycles also unfolds in three distinct stages: a rapid growth phase from 0 to 1 cycle, a slow growth phase spanning 1 to 4 cycles, and a stable phase from 4 to 5 cycles. Under an equivalent number of dry and wet cycles, the soil crack rate is consistently lower than that of the unsolidified counterpart, with a higher PAAS content correlating to a reduced crack rate. This indicates that the incorporation of PAAS effectively curtails crack development in the solidified soil. Following 5 cycles, the crack rates for varying dosages ranged from 5.78% to 6.84%, representing a 97.68% to 135.92% decrease compared to the unsolidified soil.

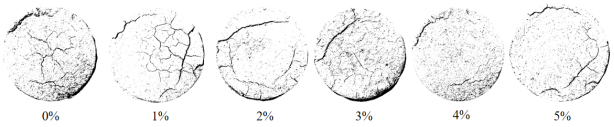

Fig. 13. Dry and wet cycling 4 times cleavage skeleton

Fig. 13 presents the crack pattern observed in the PCAS system following four cycles of dry-wet alternation Error! Reference source not found., the number of cracks and the crack area in the solidified soil are analysed using image processing techniques, by converting the captured crack images into black-and-white binary images through threshold segmentation and binarisation. PCAS is a particle (pore) and fracture image recognition and analysis system, developed by Nanjing University as a specialized tool for pore analysis. Leveraging its automated image recognition and quantitative analysis capabilities, it is widely used in various research fields, including geology and geotechnical engineering, significantly improving the efficiency and accuracy of studies related to pores and fractures. Fracture images of solidified soil can be binarized to remove noise, after which particles and pores are automatically segmented and identified, providing outputs such as the number, area, and length of particles and pores. It can also calculate key indicators such as porosity, directional probability entropy, and fractal dimension, and generate vector images that illustrate the distribution patterns and structural features of mineral particles and soil pores.

From the Fig. 13, it is evident that the unsolidified sample exhibits pronounced primary primary (Refers to the fissures that first form in the soil under wet-dry cycles, loading, or drying shrinkage stress, and play a dominant role in structural failure) and secondary cracks (Refers to branch cracks that originate from or depend on the main crack, appearing during the propagation of the main crack

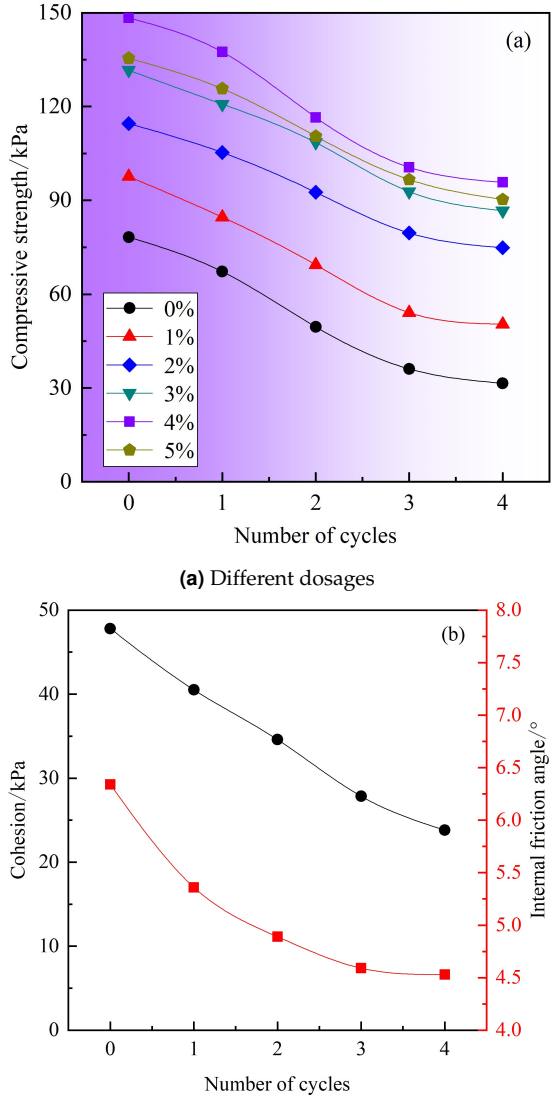

(a) Different dosages

(b) 4% PAAS Content

Fig. 14. Strength characteristics of cured soil under wet and dry cycles

and playing an auxiliary role in structural damage), which progressively cause the soil aggregates to detach from the edges. As the PAAS content increases, the reduction in both the primary crack width and the quantity of secondary cracks demonstrates a gradual suppression of crack development in the solidified soil. Once the PAAS content surpasses 4%, the extent of soil structural damage becomes minimal. In this state, the secondary cracks close upon exposure to water, leaving only the primary crack visible at the periphery.

Figs. 14a and 14b respectively depict the strength characteristics of solidified soil under different dosages and a 4% PAAS dosage after undergoing dry-wet cycling. To highlight the trend of changes, only the performance after 0 cycles (initial), 1 cycle, 3 cycles, and 4 cycles is shown. Since the performance stabilizes after 5 cycles (with no significant changes), it is omitted to avoid making the figures too complex. As shown in Fig. 14a, a negative correlation is observed between the compressive strength of the solidified soil and the number of cycles. Despite the cycling, the solidified soil exhibits superior compressive strength to the unsolidified soil. A more significant attenuation in compressive strength is noted for the solidified soil, which may be accounted for by the formation of van der Waals forces within the solidified soil after dry-wet cycling. These forces promote the aggregation of fine particles, results in a higher proportion of large particles while a reduction in specific surface area, porosity, and soil strength [29]. The rate of strength degradation gradually slows down as the cycles rises.

Fig. 14b illustrates the shear strength index of the 4% stabilized soil across different cycles. As indicated in Fig. 14b, the cohesion of the solidified soil undergoes an initial decline before plateauing with rising cycle numbers, with the most notable changes occurring during the first two cycles. This phenomenon is attributed to the significant structural damage caused by wet expansion and dry shrinkage [30]. Lee et al. [31] demonstrated that the solidified soil consistently stabilized the cohesion of soil particles throughout the drying and wetting cycles. As the cycles rises, both the cohesion and internal friction angle of the solidified soil exhibit a gradual decline. The amplitude of variation becomes relatively stable after three cycles.

3.6. Microscopic analysis of PAAS solidified expansive soil

3.6.1. SEM and XRD assay analysis

Figs. 15a and 15b present SEM images of untreated and 4% PAAS-treated expansive soil, respectively. In Fig. 15a, the untreated soil is composed mainly of aggregates and scattered, variably-sized loose particles. The presence of large pores between the relatively dispersed soil particles leads to weak particle connectivity.

Fig. 15b reveals that after PAAS treatment, the number and size of pores in the soil are significantly reduced. Additionally, there is a noticeable presence of colloidal attachments (such as hydrogels and flocculent adhesive films) on the soil particles surface. In essence, the incorporation of PAAS enhances the cohesive properties of soil particles, reduces their fluidity, strengthens the inter-particle connections, and effectively improves soil compactness. It is also observed that the soil particles are enveloped by this gel film, rendering their boundaries indistinguishable. The

high-viscosity gel forms a coating that excessively packs the particles, resulting in a small effective contact area between them. This leads to the formation of a spatial network structure, which hardens the soil and improves the soil skeleton, thereby enhancing the overall strength. This improvement is macroscopically manifested as an increase in strength characteristics.

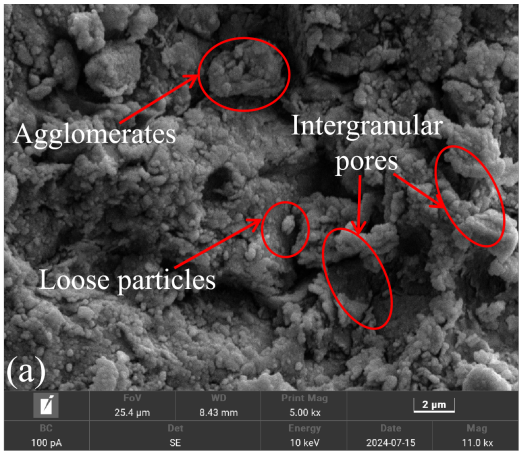

(a) Uncured

(b) 4% PAAS dosage cures

Fig. 15. SEM image of expanded soil

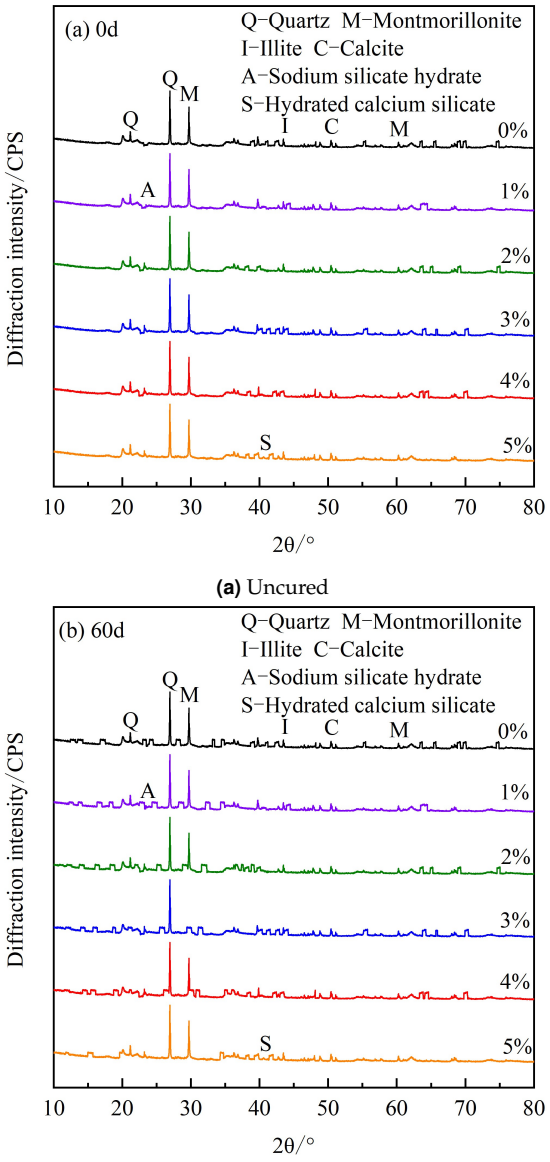

(a) Uncured

(b) 4% PAAS dosage cures

Fig. 16. XRD pattern of PAAS-cured expansive soil

Fig. 16 displays the XRD patterns of expansive soil treated with a stabilizing agent. The analysis reveals that the peak characteristics in the XRD patterns of the stabilized soil remain largely unchanged, with no new diffraction peaks observed. This indicates that the PAAS stabilization process does not lead to the formation of new crystalline minerals. The primary clay minerals identified are quartz, montmorillonite, and illite, with slight variations in their relative abundances.

Fig. 16 indicates that the content of hydrophilic minerals in the stabilized soil dropped by 43.14%(43.14% comes from the relative quantitative analysis of the change in the relative content of hydrophilic mineral characteristic peaks and internal standard peak intensity before and after curing. Its value only shows a slight change in peak intensity on the XRD spectrum, and does not obviously indicate a halving of the content.) after 60 days of curing. This reduction is a direct result of the significant SiO content inherent to the expansive soil. Upon hydration, SiO_2 reacts to form silicate species, facilitating the presence of $K^+$and Na^+ions within the interlayers of montmorillonite crystals [32]. However, when PAAS dissolves in water, it releases a significant number of $OH^-$and $CHOO^-$ (formate) ions. These anions participate in cation exchange reactions with the interlayer K^+ and Na^+ions in montmorillonite [33].

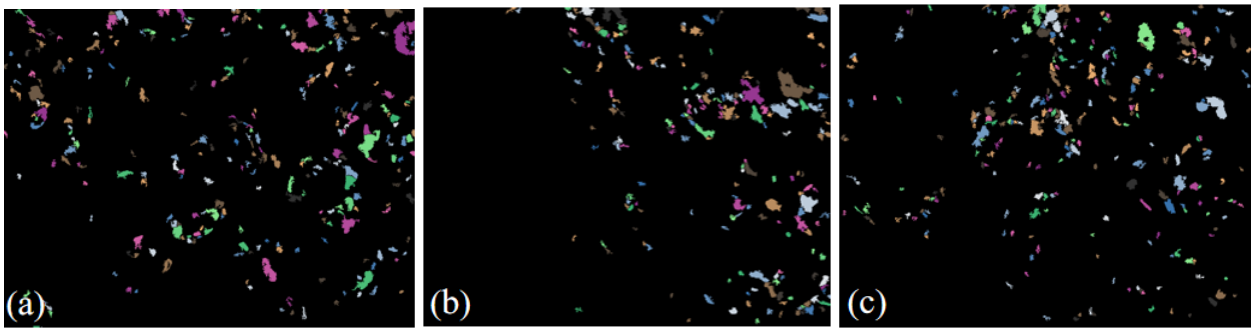

(a) 0% for PAAS **(b)** 1% for PAAS **(c)** 2% for PAAS

(d) 3% for PAAS **(e)** 4% for PAAS **(f)** 5% for PAAS

Fig. 17. Pore space of cured soil

The resulting formation of soluble hydration products such as $NaHCO_3$ contributes to the suppression of soil expansion by reducing the osmotic potential and weakening the swelling capacity of the clay minerals.

3.6.2. PAAS pore size analysis of solidified expansive soil

To study the particle pore size of solidified soil, the PCAS porosity analysis software developed by Nanjing University [34] was used for quantitative analysis of SEM images. PCAS, which stands for Particle (Porosity) and Fracture Image Recognition and Analysis System, is a professional porosity analysis tool developed by Nanjing University. With its automated image recognition and quantitative analysis capabilities, it automatically segments and identifies particles and pores, outputting key indicators such as the number, area, length, porosity, orientation probability entropy, and fractal dimension of particles and pores, and generates results in vector images and rose diagrams. Threshold segmentation was applied to the SEM images for fracture statistical analysis between particles.

After repeated adjustments, a threshold value of 40 achieved better segmentation results, with a fixed pore throat radius of 2 and a minimum area of 50. Fig. 17 shows the pore image of solidified soil cured for 60 days (black in the figure represents the soil matrix, and colored areas represent pores).

As illustrated in Fig. 17, in the absence of PAAS, the specimen exhibits large internal pores and loosely packed soil particles, leading to low strength, significant water absorption, expansion, and contraction. Upon the incorporation of PAAS, the soil pores undergo varying degrees of modification, with the solidified soil overall porosity effectively reduced. Due to the excellent binding capacity of PAAS with soil particles, the formation of aggregates and hydrates fosters intimate intermingling among soil particles, enhances particle-to-particle contact forces, and substantially improves strength. However, when the PAAS content surpasses 4%, the total porosity of the solidified soil begins to rise, compromising the soil's integrity and resulting in a gradual decline in strength. This trend mirrors the variations observed in compressive and shear strength, reinforcing the notion that a 4% PAAS dosage yields the optimal curing effect.

Table 3 presents the fracture parameters derived from SEM images after 60 days of curing. According to the data in Table 3, the maximum length of the cured soil exceeds that of the uncured soil, highlighting the effective role of the curing agent in enhancing soil stretching. Moreover, a higher fracture curvature coefficient in the cured soil signifies improved resistance to deformation, indicating that the solidified soil possesses excellent ductility, manifesting in larger widths and lengths during fracture and

Table 3. Crack parameter results for cured soil

Dosage /%	Maximum length	Maximum width	Curvature coefficient	Crack rate /%
0	88.64	45.01	1.06	5.56
1	98.06	52.77	1.03	5.11
2	71.6	44.6	1.12	4.58
3	133.71	48.59	1.12	3.69
4	102.02	71.74	1.22	3.08
5	112.4	62.69	1.27	5.13

deformation resistance processes. The porosity of the cured soil exhibits an initial decrease followed by an increase, with the minimum crack width observed at a 4% PAAS content. This observation underscores that the curing effect is most pronounced at this concentration, fostering a tightly interwoven intergranular structure that aligns with the principles of mechanical expansion.

3.6.3. PAAS Microscopic mechanism of PAAS curing expansive earth

Fig. 18 shows the mechanism of PAAS solidification of expansive soil. Expansive soils are originally rich in a large number of free and dispersed hydrophilic minerals (typically montmorillonite), which are saturated with aqueous solution and highly porous. When PAAS is introduced, the hydroxyl groups in its molecular chain interact with water molecules to induce the formation of hydrogen bonds, and this chemical reaction promotes the conversion of PAAS polymer monomers into viscous gel films. The gel film not only fills the pores and wraps the soil particles, but also shows strong cementing ability, effectively reducing the aqueous solution content and pore volume in the soil, thereby yielding a densified soil configuration (Fig. 18(b)).

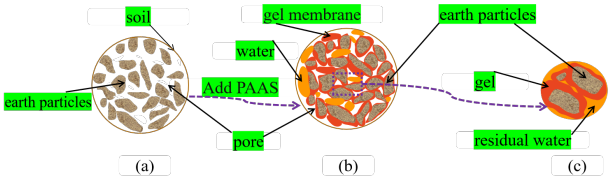

Fig. 18. Schematic diagram of PAAS cured expansive soil

Furthermore, PAAS gel membranes also enhance the function of the gel membrane by enhancing the double layer effect between particles, and more effectively adsorb and encapsulate those originally free and dispersed soil particles [10]. Therefore, the gel film formed by PAAS polymers is embedded inside the soil, which not only cements and envelops fine soil particles, but also promotes the formation of more stable aggregates of these particles, as shown in Fig. 18 [35]. This series of changes not only adjusts the arrangement and distribution of soil particles, but also constructs a more stable soil structure, which significantly improves the mechanical properties of expansive soil.

3.7. Analysis of the 'Performance-Economic' Relationship of PAAS-Stabilized Expansive Soil

As a water-soluble polymer material, PAAS demonstrates unique technical advantages in the solidification of expansive soil. However, based on the 'technical performance-cost matching', a 'performance-economic' correlation analysis is conducted by combining the results of laboratory tests with the cost characteristics on site:

(1) Experiments show that a 5% addition of PAAS can reduce the free expansion rate by 53.82% and the unloaded expansion rate by 56.37%, with the expansion stabilized within 60 days, keeping the free expansion rate below 40%. This advantage is particularly valuable for emergency projects that require rapid suppression of expansive soil deformation, such as temporary roads and foundation pit slopes. Traditional cement stabilization requires 28 days of standard curing to stabilize expansion, whereas PAAS can achieve short-term stabilization by quickly encapsulating hydrophilic minerals with a gel membrane, reducing the construction period by more than 50%. The mentioned $0.8 \sim 1.2\%$ refers to the proportion of the active component in the PAAS molecule relative to the dry soil mass. Because industrial-grade PAAS solid powder contains a small amount of impurities (such as sodium chloride and unreacted monomers, accounting for about $5 \sim 8\%$), its actual utilisation efficiency in soil dissolution and diffusion is much lower than the total added powder. An addition of 4% powder corresponds to an effective active component proportion of about $1.0 \sim 1.1\%$, which is precisely within the $0.8 \sim 1.2\%$ control range. This illustrates the relationship between the total amount added and the effective amount used.

(2) By controlling the amount, a 'performance peak-cost optimal' match can be achieved. If the dosage exceeds 4%, not only will the mechanical properties decline (e.g., compressive strength drops, main fractures develop), but material consumption and transportation costs will also

increase [36]. If it is below 0.8%, curing is insufficient (shear strength improvement $< 15\%$), requiring secondary reinforcement and resulting in additional costs.

(3) PAAS relies on a microscopic mechanism of forming a gel membrane to fill pores and reduce cracks, depending on pre-treatment conditions of 'soil particle size < 5 cm and moisture content $18 \sim 22\%$'. In alkaline areas with pH > 8.5, PAAS still exhibits high ion exchange efficiency, and in arid regions with an average annual precipitation of less than 400 millimeters, its water-retention properties can provide moisture for plant growth [37].

(4) After curing with 4% PAAS, the compressive strength increased by $31\% \sim 105\%$, and the 60 -day free swelling rate was less than 40%. For soil cured with 15% cement, the 28 -day compressive strength increased by $120\% \sim 180\%$, and the free swelling rate decreased by $40\% \sim 60\%$. The carbon emissions after PAAS curing are $40\% \sim 50\%$ lower than those of cement, and the carbon trading revenue can cover $15\% \sim 20\%$ of the total cost. Cement curing produces high carbon emissions during production (about 0.8 tons of CO_2 per ton of cement). The cost-benefit ratio of PAAS-cured soil is 1:2.3, lower than that of cement-cured soil, which is 1:3.1. Considering the carbon reduction benefits, its environment-adjusted cost-benefit ratio can increase to 1:2.8 [38]. This characteristic gives PAAS-cured soil significant application value in ecologically sensitive areas or regions where carbon trading is mature.

4. Conclusions

Laboratory experiments examined the influence of PAAS on the volume change and mechanical characteristics of expansive soil. Furthermore, the solidification process of PAAS on expansive soil was clarified using SEM and XRD analyses at a microscopic scale. The key discoveries are summarized below:

(1) The application of PAAS leads to a effective reduction in the liquid limit and plasticity index, alongside an elevation of the plastic limit in the treated soil. In particular, the free expansion rate of soil cured with 5% PAAS dropped by 53.82%, staying under 40% after 60 days of curing, which shows a notable decrease in expansion. Additionally, the unloaded expansion rate of the 5% solidified soil was reduced by 56.37%, and the loaded expansion rate decreased by between 35% and 93%.

(2) An initial increase in the compressive strength of the solidified soil with PAAS content is observed, reaching a maximum at 4%, followed by a subsequent decrease. The material shows a compressive strength increase of 31% to 105%. Similarly, the E_{50} value exhibits an initial increase and then a decline as the PAAS dosage rises. After prolonged curing, the solidified soil showed an 88.93% increase in its resistance to deformation.

(3) The shear strength of the solidified soil increases linearly with increasing normal stress. After curing, the maximum shear strength reaches 216.02 kPa , representing a 261.78% improvement relative to the uncured state. Both the friction angle and cohesion of the solidified soil initially increase and subsequently decrease with higher PAAS content, with maximum increases of 137.74%, respectively.

(4) The incorporation of PAAS reduces both the width and number of cracks in the solidified soil, effectively suppressing crack propagation. The minimum crack ratio is observed at a PAAS content of 4%. The compressive strength, cohesion, and internal friction angle of the solidified soil decrease as the number of loading cycles increases. The degree of soil structure degradation increases slightly once the PAAS content exceeds 4%, with the primary fissure developing at the occluded edges of secondary cracks upon exposure to water.

(5) The incorporation of PAAS reduces the number of pores and the crack rate in the solidified soil. XRD analysis shows a 43.14% reduction in hydrophilic minerals. PAAS and aqueous solutions promote hydrogen bonding between water molecules via hydroxyl groups in the molecular chain, facilitating the development of a viscous gel film. This film provides filling, encapsulation, and binding effects, effectively reducing moisture content and pore spaces of the soil, thereby enhancing its density and compactness.

5. Acknowledgments

The authors want to thank the editor and anonymous reviewers for their valuable suggestions for improving this paper.

References

[1] W.-m. Ye, L.-w. Kong, R.-l. Hu, F.-s. Zha, S.-w. Shi, and Z.-r. Liu, (2022) *"Research on New Prevention and Control Techniques and Engineering Demonstration of Expansive Soil Landslides and Engineering Slopes"* **Chinese Journal of Geotechnical Engineering *44***(07): 1295–1309. DOI: 10.11779/CJGE202207009.

[2] F. Kewei, J. Haoze, L. Jianguo, Y. Jun, and W.-l. Zou, (2022) *"Effect of the history of drying-wetting cycles on the deformation of expansive soils in seasonal frost region"* **Zhongnan Daxue Xuebao (Ziran Kexue Ban)/Journal of Central South University (Science and Technology) *53***: 280–287. DOI: 10.11817/j.issn.1672-7207.2022.01.022.

[3] D. Wang, Z. Zhang, and X. Wang, (2022) *"Performance and Micromechanism of Cement-Modified Expansive Soils under the Influence of Freeze-Thaw and Dry-Wet Cycles"* **Journal of Central South University: Science and Technology *53***(01): 306–316. DOI: 10.11817/j.issn.1672-7207.2022.01.025.

[4] M. Wang, S. Qin, J. Li, and P. Xu, (2014) *"Strength of unsaturated lime-treated expansive clay in Hefei"* **Chinese Journal of Rock Mechanics and Engineering *33***(S2): 4233–4238. DOI: 10.13722/j.cnki.jrme.2014.s2.104.

[5] X. Fu, J. Wang, and G. Zhang, (2017) *"Experimental study about mechanic and permeability of soil-cement in different pH value"* **Journal of Railway Science and Engineering *14***(08): 1639–1646. DOI: 10.19713/j.cnki.43-1423/u.2017.08.010.

[6] Y. Shang, L. Xu, and Y. Cai, (2019) *"Dynamic Characteristics of Cement-Improved Expansive Soil Subgrade under Cyclic Dynamic Load of Heavy Haul Railway"* **China Railway Science *40***(06): 19–29. DOI: 10.3969/j.issn.1001-4632.2019.06.03.

[7] T. Wang, L. Wang, and S. Liu, (2023) *"Experimental Study on Mechanical Properties of Expansive Soil Improved by Xanthan Gum and Guar Gum"* **China Railway Science *44***(02): 1–10. DOI: 10.3969/j.issn.1001-4632.2023.02.01.

[8] S. Naveena and D. Reddy. "Strength Characteristics of Expansive Soils Using Eco-Friendly Xanthan Gum". In: 2017.

[9] N. Keshav, A. Prabhu, and A. Kattimmani. "Enhancing the Properties of Expansive Soil Using Biopolymers-Xanthan Gum and Guar Gum". In: 2019. DOI: org/10.1007/978-981-33-6564-3-12.

[10] U. Ou, H. Zhang, and R. Deng, (2025) *"Study on Development of Cracks in Expensive Soil Improved by Xanthan Gum Biopolymer"* **Chinese Journal of Geotechnical Engineering *47***(01): 106–114. DOI: 10.11779/CJGE20230989.

[11] J. Xiao, Y. Liu, and D. Wang, (2023) *"Experimental study on engineering characteristics of composite improvement of expansive soil by using microbial technology"* **Chinese Journal of Geotechnical Engineering *45***(S1): 97–101. DOI: 10.11779/CJGE2023S10047.

[12] H. Liu, D. Li, and B. Hu, (2022) *"Experimental Study on Improving the Swelling Characteristics of Expansive Soil Using MICP Technology"* **Journal of Yangtze River Scientific Research Institute *39***(06): 150–156. DOI: 10.11988/ckyyb.20220049.

[13] H. Wang, J. Zhang, and H. Guo, (2024) *"Experimental study on physical and mechanical properties of expansive soil improved by EICP"* **Journal of Civil and Environmental Engineering *46***(05): 109–116. DOI: 10.11835/j.issn.2096-6717.2023.130.

[14] N. Latifi, S. Horpibulsuk, C. L. Meehan, M. Z. A. Majid, M. M. Tahir, and E. T. Mohamad, (2016) *"Improvement of Problematic Soils with Biopolymer—An Environmentally Friendly Soil Stabilizer"* **Journal of Materials in Civil Engineering *29***(2): 04016204–04016204. DOI: 10.1061/(ASCE)MT.1943-5533.0001706.

[15] I. Chang, J. Im, and G.-C. Cho, (2016) *"Introduction of Microbial Biopolymers in Soil Treatment for Future Environmentally-Friendly and Sustainable Geotechnical Engineering"* **Sustainability *8***(3): 251. DOI: 10.3390/su8030251.

[16] I. G. Panova, A. A. Kiushov, D. D. Khaydapova, S. B. Zezin, M. S. Arzhakov, and A. A. Yaroslavov, (2021) *"A dramatic change in rheological behavior of a clay material caused by a minor addition of hydrophilic and amphiphilic polyelectrolytes"* **Polymers *13***(21): 3662. DOI: 10.3390/polym13213662.

[17] H. R. Khatami and B. C. O'Kelly, (2013) *"Improving Mechanical Properties of Sand Using Biopolymers"* **Journal of Geotechnical and Geoenvironmental Engineering *139***(8): 1402–1406. DOI: 10.1061/(ASCE)GT.1943-5606.0000861.

[18] M. A. Kumar, A. A. B. Moghal, R. M. Rasheed, and A. U. Rehman, (2025) *"Enhancing durability and erosion resistance of soils with varying plasticity using crosslinked biopolymers"* **Scientific Reports *15***(1): 12572–12572. DOI: 10.1038/S41598-025-96977-6.

[19] H. Fatehi, S. M. Abtahi, and H. Hashemolhosseini, (2018) *"A novel study on using protein based biopolymers in soil strengthening"* **Construction and Building Materials *167***: 813–821. DOI: 10.1016/j.conbuildmat.2018.02.028.

[20] C. Zhu, P. Yu, Z. Guo, Q. Wang, and H. Liu, (2025) *"Mechanical Properties and Microstructure Characteristics of Submerged Cement-Based Stabilized Marine Soft Clay Enhanced with ISS and PAM"* **Journal of Ocean University of China *24***(2): 387–403. DOI: 10.1007/S11802-025-5861-8.

[21] J. Liu, B. Shi, H. Jiang, S. Bae, and H. Huang, (2009) *"Improvement of water-stability of clay aggregates admixed with aqueous polymer soil stabilizers"* **Catena *77***(3): 175–179. DOI: 10.1016/j.catena.2008.12.016.

[22] M. Santos, S. Rebola, and D. V. Evtuguin, (2025) *"Soil Remediation: Current Approaches and Emerging Bio-Based Trends"* **Soil Systems *9***(2): 35–35. DOI: 10.3390/SOILSYSTEMS9020035.

[23] J. Wang, H. Liu, and Z. Lin, (2024) *"Experimental study on engineering properties of red clay modified by sodium polyacrylate"* **Hydrogeology & Engineering Geology *51***(03): 110–117. DOI: 10.16030/j.cnki.issn.1000-3665.202305036.

[24] H. Chen, S. Niu, and S. Feng, (2025) *"Engineering properties and microstructure of sodium polyacrylate modified calcium bentonite"* **Chinese Journal of Geotechnical Engineering *47***(04): 860–868. DOI: 10.11779/CJGE20240103.

[25] F. Yang, Y. Zhao, H. Dong, and H. Wang, (2025) *"Mechanical and microscopic characterization of expansive soils modified by water-soluble polymers."* **Scientific reports *15***(1): 2315. DOI: 10.1038/S41598-025-85395-3.

[26] X. Bian, L. Zeng, and X. Li, (2021) *"Fabric changes induced by super-absorbent polymer on cemente-lime stabilized excavated clayey soil"* **Journal of Rock Mechanics and Geotechnical Engineering *13***(05): 1124–1135. DOI: 10.1016/J.JRMGE.2021.03.006.

[27] M. of Transport of the People's Republic of China. *Test Methods of Soils for Highway Engineering*. 2007.

[28] J. ZHANG, X. ZHAO, and T. JIANG, (2022) *"Water retention characteristics of silt improved by three types of biopolymer"* **Rock and Soil Mechanics *43***(08): 2157–2164. DOI: 10.16285/j.rsm.2022.0021.

[29] Z. HU, W. YE, Q. WANG, and Y. CHEN, (2025) *"A Review on the Microstructural Characteristics of Montmorillonite and Its Water Adsorption Mechanisms"* **Chinese Journal of Geotechnical Engineering**: 1–10. DOI: 10.11779/CJGE20250275.

[30] L. LI, C. HUANG, and W. LI, (2023) *"Study on mechanical and microscopic characterization of expensive soil solidified by rice husk ash-granulated blast furnaxe slag"* **Rock and Soil Mechanics *44***(10): 2821–2832+2842. DOI: 10.16285/j.rsm.2023.0740.

[31] S. Lee, I. Chang, and M.-K. Chung, (2017) *"Geotechnical shear behavior of Xanthan Gum biopolymer treated sand from direct shear testing"* **Geomechanics and Engineering *12***(5): 831–847. DOI: 10.12989/GAE.2017.12.5.831.

[32] M. Qiang, H. Zeli, H. Zhi, and L. Junhui, (2022) *"Strength characteristics and micro-scale mechanism of high liquid limit clay treated by recycled construction and demolition wastes (CDW) aggregates"* **Construction and Building Materials *332***: DOI: 10.1016/J.CONBUILDMAT.2022.127367.

[33] W. Z. yu, Y. Jin, D. Y. feng, C. Y. yan, and W. L. na, (2023) *"Mechanical behavior and strengthening mechanism of red clay solidified by xanthan gum biopolymer"* **Journal of Central South University *30***(6): 1948–1963. DOI: 10.1007/S11771-023-5327-3.

[34] C. LIU, Q. XU, and B. SHI, (2018) *"Digital image recognition method of rock particle and pore system and its application"* **Chinese Journal of Geotechnical Engineering *40***(05): 925–931. DOI: 10.11779/CJGE201805018.

[35] R. ZHANG, M. LONG, and T. LAN, (2020) *"Stability analysis method of geogrid reinforced expansive soil slopes and its engineering application"* **Journal of Central South University *27***(07): 1965–1980. DOI: 10.1007/s11771-020-4423-x.

[36] A. Ahmad, U. Khalid, and Z. ur Rehman, (2025) *"Reclaimed brick masonry waste recycling in macro–micro amelioration of cemented clayey soil: an eco-friendly construction waste solution"* **Journal of Material Cycles and Waste Management *27***(2): 1–22. DOI: 10.1007/S10163-025-02161-3.

[37] T. Ben-Gang, C. Qing, T. Chao-Sheng, and Z. Hao, (2022) *"Effects of compaction state on desiccation cracking behaviour of a clayey soil subjected to wetting-drying cycles"* **Engineering Geology *302***: DOI: 10.1016/J.ENGGEO.2022.106650.

[38] M. T. Zumstein, A. Schintlmeister, and T. F. Nelson, (2018) *"Biodegradation of synthetic polymers in soils: Tracking carbon into CO2 and microbial biomass"* **Science Advances *4***(7): eaas9024. DOI: 10.1126/sciadv.aas9024.